An Estimation-Based Precipitation Retrieval Algorithm for Attenuating Radars

TRISTAN S. L'ECUYER AND GRAEME L. STEPHENS

Department of Atmospheric Science, Colorado State University, Fort Collins, Colorado

(Manuscript received 5 February 2001, in final form 1 September 2001)

ABSTRACT

A new method for retrieving rainfall profiles from a spaceborne radar is introduced. As a result of the frequencies necessary in spaceborne radar applications, attenuation by both rainfall and liquid cloud particles is nonnegligible and must be accurately accounted for before quantitative rainfall estimates can be made. The proposed method is based on the minimization of a cost function that allows one to account for attenuation at each level directly in the iteration process. In addition, the algorithm does not invoke the Rayleigh approximation and is, therefore, applicable at wavelengths characteristic of spaceborne radars. The method is flexible with regard to the parameters to be retrieved and is well-suited for the addition of measurements from other sensors, such as a passive microwave radiometer, to constrain the retrieval. Preliminary results, using simplified assumptions of drop size distribution and particle shape, illustrate the utility of the algorithm provided the attenuation is not severe. At the frequency of the Tropical Rainfall Measuring Mission (TRMM) precipitation radar (14 GHz), synthetic retrievals are accurate to within 20% for rain rates up to 40 mm h^{-1}. On the other hand, at 94 GHz, the frequency of the CloudSat cloud profiling radar, attenuation effects are too severe at rain rates greater than 1.5 mm h^{-1}, suggesting the need for additional information to constrain the retrieval. Such information might come in the form of a path-integrated attenuation (PIA) derived from surface echo measurements or, alternatively, a precipitation water path (PWP) estimate from a passive microwave radiometer. Addition of a simple PWP constraint yields improvements in the retrieved rainfall profiles from both instruments when attenuation is severe. At 94 GHz, in particular, it is found that accurate quantitative rainfall estimates can be made provided the near-surface rain rate does not exceed 10 mm h^{-1}.

1. Introduction

Latent heat released by precipitation accounts for 75% of the heat transfered from the surface to the atmosphere (Simpson et al. 1996), and precipitation is intimately connected with both large- and small-scale circulations in the atmospheres and oceans. Of all environmental parameters, rainfall plays one of the most significant roles in global heat and water budgets, yet a lack of accurate rainfall information persists over vast areas of the globe. The presence of large oceanic regions, deserts, and jungle, particularly in the Tropics where two-thirds of all precipitation falls, precludes the use of rain gauge and other ground-based rainfall measurements in these regions. As a result, spaceborne instruments provide the only means of obtaining global measurements of rainfall (Simpson et al. 1988).

Numerous techniques based on satellite measurements of microwave emission have achieved some success in mapping global rainfall [see, e.g., Wilheit et al. (1977); Spencer et al. (1989); Kummerow and Giglio (1994); Smith et al. (1994); Petty (1994a,b)]. One drawback to these methods, however, is that few are capable of accurately determining the vertical structure of precipitation at the resolution required in global weather and climate models (e.g., Cess et al. 1993; Wang et al. 1996). In addition, such methods suffer from nonuniqueness resulting from the fact that substantially different profiles of precipitating liquid and ice hydrometeors in the atmospheric column yield similar microwave radiance signatures introducing a substantial element of uncertainty in their surface rain-rate estimates.

The profiling capabilities of spaceborne radars have the potential to add vertical structure information to complement techniques based on passive measurements. As a result, the Tropical Rainfall Measuring Mission (TRMM) carried the first radar designed for precipitation measurements flown in space. Given the success of the 14-GHz precipitation radar (PR), which has been operational for more than 3 yr, future spaceborne radar missions are being discussed. The potential for extensive spatial coverage offered by satellite-based radars has also been recognized by the CloudSat science team (Stephens et al. 2000, manuscript submitted to *Bull. Amer. Meteor. Soc.*), and a 94-GHz cloud profiling radar (CPR) will be flown on that satellite, which may be capable of measuring light rainfall in addition to clouds. As a result of the logistics of flying a radar in space,

Corresponding author address: Dr. Tristan S. L'Ecuyer, Department of Atmospheric Science, Colorado State University, Fort Collins, CO 80523-1371.
E-mail: tristan@atmos.colostate.edu

most notably size, weight, and power restrictions, only frequencies greater than 10 GHz are practical for a spaceborne radar system (Fujita and Satake 1997). Consequently, all spaceborne radars are subject to significant attenuation by the rain and clouds they are measuring, necessitating new radar-rainfall retrieval algorithms that explicitly account for attenuation effects. Hitschfeld and Borden (1954) were the first to propose a method for directly correcting measured reflectivities for attenuation. Since then, numerous retrieval schemes have been developed that incorporate aspects of this early work along with the more recent technique of constraining retrievals using path-integrated attenuation (PIA) derived from surface return echoes. Iguchi and Meneghini (1994), Marzoug and Amayenc (1994), and Amayenc et al. (1996) describe many such algorithms and evaluate them in the context of airborne and spaceborne operation.

Many ground-based radar retrieval algorithms are based on the Rayleigh approximation that the rain drops are small with respect to the radar wavelength and assume some drop size distribution (DSD) to derive a simple relationship between radar reflectivity and rain rate. From an operational standpoint these algorithms are computationally efficient, relatively simple to implement, and produce useful results but they can incur uncertainties that are difficult to estimate as a result. Errors associated with the assumption of an idealized size distribution were pointed out by Wexler (1948); Gunn and East (1954) showed that the Rayleigh approximation is not valid for wavelengths less than 3 cm (or frequencies greater than 10 GHz), emphasizing the need for an algorithm that is not restricted by such assumptions in spaceborne applications. This has been recognized by the designers of the TRMM PR rainfall profile algorithm who select a DSD based on rain type and the presence or absence of a bright band and correct the DSD based on a PIA estimate (Iguchi et al. 2000).

Another shortcoming of many algorithms is their inability to adapt measurements from other instruments except in a limited capacity. With the growing trend toward multisensor platforms as exemplified by the TRMM satellite, it is important to develop algorithms better suited to combining information from a variety of different sources simultaneously in rainfall retrievals. Again, this has been recognized by the TRMM science team and a first-generation combined PR–TRMM Microwave Imager (TMI) rainfall algorithm has been developed, which employs a Bayesian approach to retrieve DSD parameters from PR reflectivities with a PIA estimate derived from the 10.6-GHz channel of the TMI (Haddad et al. 1997).

Rigorous estimates of the uncertainty in the retrieved rainfall profiles are required for model validation and data assimilation applications, but many algorithms are limited to a rough estimate of their accuracy. For this reason, all operational TRMM algorithms, including the two PR algorithms described above, are required to provide estimates of their accuracy, and considerable emphasis will be placed on error diagnostics for the algorithm presented below.

This paper presents a complete algorithm for retrieving profiles of rainfall from spaceborne radar measurements that seeks to address these issues and provide an alternate method of inversion to either of those currently employed in the TRMM algorithms. This new algorithm differs from those of many previous works in that it can be adapted to use any DSD, requires no simplifying assumptions regarding particle shape provided that backscatter information can be computed, and is readily modified to include any additional measurements that are available. Section 2 introduces a general model for computing radar reflectivities for any profile of atmospheric particles. A detailed description of the inversion method is presented in section 3, and results of some synthetic retrievals are discussed in section 4. The utility of adding a simple total liquid water path constraint is demonstrated in section 5.

2. Attenuating radar forward model

In general, the return power P_r received by a radar, which transmits a power P_t at wavelength λ is given by

$$P_r = \left[\frac{P_t G^2 \lambda^2 \theta \phi h}{512(2\ \ln 2)\pi r^2}\right] \exp\left[-2 \int_0^r k_{\text{ext}}(s)\ ds\right] \eta, \quad (1)$$

where G is the antenna gain, θ and ϕ characterize the half-power beamwidth of the pulse, h is the length of the emitted pulse, and r is the range to the target. With k_{ext} defined as the attenuation coefficient, the exponential factor accounts for the two-way attenuation due to all atmospheric constituents along the slant path s of the radar beam. Last, η is the radar reflectivity per unit volume V given by

$$\eta = \int_V \sigma_b\ dV, \quad (2)$$

where the σ_b are the backscatter cross sections (per unit volume) of the particles in the target volume.

Many ground-based radar models assume that the particles in the target volume are much smaller than the wavelength of the incident radiation $\pi D/\lambda \ll 1$ and use the Rayleigh approximation for the backscatter cross-section yielding

$$\eta = \frac{\pi^5}{\lambda^4} |K|^2 Z, \quad (3)$$

where $Z = \int D^6 N(D)\ dD$ is the Rayleigh reflectivity factor and $K = (m^2 - 1)/(m^2 + 2)$ is the dielectric factor of the scattering target. Here $N(D)\ dD$ is used to denote the number of particles with diameters between D and $D + dD$ in the target volume, and $m = n - ik$ is the wavelength and temperature-dependent complex refractive index of the scatterers. At the frequencies used in

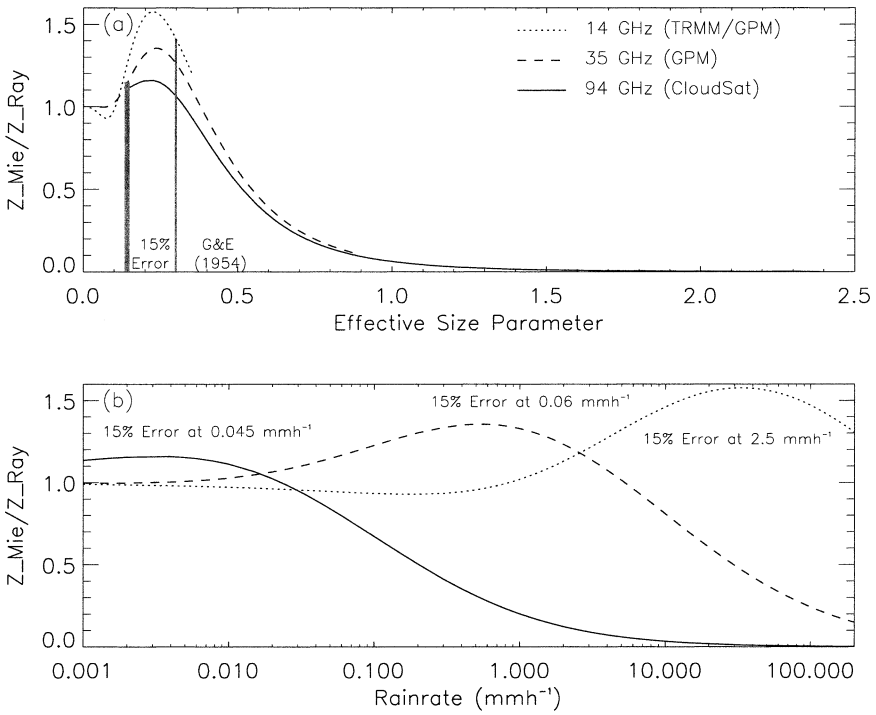

FIG. 1. Ratio of effective reflectivity computed using Mie theory to Rayleigh reflectivity as a function of (a) effective size parameter and (b) rain rate.

most spaceborne applications, the Rayleigh approximation breaks down in rain. Figure 1a illustrates the ratio of Mie to Rayleigh reflectivity factors at 14, 35, and 94 GHz as a function of size parameter $\chi = \pi D/\lambda$, assuming spherical liquid raindrops distributed according to the DSD of Marshall and Palmer (1948, hereinafter referred to as MP). Plotted in this way, the frequency dependence of the ratio can be attributed solely to differences in the real part of the refractive index, which is greatest at 14 GHz and lowest for 94 GHz. The results show that using the Rayleigh approximation leads to large errors for size parameters greater than about 0.15 when integrating over a size distribution. Cast as a function of rainfall rate in Fig. 1b, the Rayleigh approximation is only suitable for rain rates less than 2.5 mm h^{-1} at 14 Ghz and is not applicable in any appreciable rainfall at 35 or 94 GHz.

Based on these results, a more general form for the reflectivity η is adopted:

$$\eta = \int_V \sigma_b \, dV = \frac{1}{4} \int Q_{\text{sca}} P(\Theta = 180) \pi D^2 N(D) \, dD, \quad (4)$$

where $P(\Theta = 180)$ is the scattering phase function evaluated in the backscatter direction, Q_{sca} is the scattering efficiency equal to the ratio of the particle's scattering cross section to its geometric cross section, and $N(D)$ is an arbitrary number distribution of particles as a function of their effective diameter D. A series of tables of $P(\Theta = 180)$ and Q_{sca} are created as a function of particle size using Mie theory for spherical particles or some alternate computational method for more complicated particle shapes. This allows flexibility with regard to particle size, shape, and number concentration, all of which can be adapted to any given problem as needed.

Combining Eqs. (1), (3), and (4), a model to simulate an effective radar reflectivity factor for any atmospheric profile is constructed:

$$Z_{\text{eff}} = \exp\left[-2 \int_0^r k_{\text{ext}}(s) \, ds\right] \times \frac{\lambda^4}{4\pi^5 |K|^2} \int Q_{\text{sca}} P(\Theta = 180) \pi D^2 N(D) \, dD. \quad (5)$$

Unattenuated reflectivities are computed at each level, along with an attenuation correction due to the hydrometeors in that level. Each reflectivity is then corrected in turn for the attenuation through the levels above it.

3. Optimal estimation approach to inversion

Many radar algorithms assume a size distribution and Rayleigh scattering to obtain relations of the form $Z = aR^b$ and $k = \alpha R^\beta$, which are directly invertible to obtain rain rate given radar reflectivity measurements. These methods have the advantage that they cast the problem

into a simple analytical form, which results in a computationally quick and relatively simple retrieval algorithm. These assumptions also lead to two potential sources of uncertainty: 1) the assumption of a DSD strongly influences the values of a, b, α, and β, and 2) the Rayleigh assumption is not valid for radars with frequencies in excess of 10 GHz, a characteristic of both the TRMM PR and CloudSat CPR. In the present work, a significantly different technique is applied to invert Eq. (5) based on the works of Rodgers (1976, 1990) and Marks and Rodgers (1993) and applications of their work by Engelen and Stephens (1999) and Miller et al. (2000). Within the constructs of this approach a high degree of generality is maintained, which allows one to vary assumed particle size and shape and facilitates the addition of complementary information from different sensors if so desired.

a. Basic theory

Denoting the forward model in the previous section by F, a general profile of radar reflectivities $\mathbf{Z}$ can be expressed as

$$\mathbf{Z} = F(\mathbf{R}, \mathbf{b}) + \boldsymbol{\epsilon}_Z, \tag{6}$$

where $\boldsymbol{\epsilon}_Z$ is a vector of measurement uncertainties. For the purpose of illustrating the method, we cast the retrieval in terms of the vertical profile of rain rate $\mathbf{R}$ (mm h^{-1}), representing all other parameters in the radar forward model by $\mathbf{b}$. This choice is purely arbitrary and the algorithm could, equivalently, be developed in terms of any other set of parameters that completely describe the DSD. An alternate formulation may be particularly useful when other observations are available to supplement the reflectivities to constrain the shape of the size distribution. In either case, an appropriate F to be used in the retrieval can be selected from criteria such as rain type, freezing level, or the presence of a bright band and uncertainties in the parameter vector $\mathbf{b}$ must be explicitly accounted for in the inversion approach.

Our problem is to estimate the rain-rate profile that most likely produced a given observed profile of reflectivity. Following Olson et al. (1996), the optimal rain-rate profile is given by

$$E(\mathbf{R}) = \int \mathbf{R}\,\mathrm{pdf}(\mathbf{R})\, d\mathbf{R}, \tag{7}$$

where pdf($\mathbf{R}$) is a probability density function proportional to the conditional probability that $\mathbf{R}$ is the true atmospheric rain-rate profile given the observed reflectivity profile $P(\mathbf{R} = \mathbf{R}_{\text{true}} \mid \mathbf{Z}_{\text{true}} = \mathbf{Z})$. Invoking Bayes's theorem, the probability density function can be recast as a product of the probability of observing a reflectivity profile $\mathbf{Z}$ given a simulated reflectivity profile, $F(\mathbf{R})$, and the a priori probability that $\mathbf{R}$ is the true rain-rate profile,

$$\mathrm{pdf}(\mathbf{R}) \propto P[\mathbf{Z} \mid F(\mathbf{R})]P_a(\mathbf{R}). \tag{8}$$

Jaynes (2001) argues that, according to the principle of maximum entropy, the Gaussian distribution is the ''most honest'' representation of errors if only the mean and variance of a probability distribution are known. Alternate distributions, unless rigorously justifiable, add spurious information to the retrieval, therefore biasing the results. For this reason, uncorrelated and unbiased Gaussian statistics will be adopted to ensure that only distribution mean and variance information are introduced in the retrieval. Under this assumption,

$$P[\mathbf{Z} \mid F(\mathbf{R})] \propto \exp\left\{-\frac{1}{2}[F(\mathbf{R}) - \mathbf{Z}]^{\mathrm{T}}\mathbf{S}_Z^{-1}[F(\mathbf{R} - \mathbf{Z})]\right\}, \tag{9}$$

where $\mathbf{S}_Z$ is the total error covariance matrix representing the sum of the measurement and model errors. Similarly, if $\mathbf{R}_a$ represents some a priori guess at a rain-rate profile, the probability of finding the true atmospheric rain-rate profile $\mathbf{R}$ will be expressed as

$$P_a(\mathbf{R} \mid \mathbf{R}_a) \propto \exp\left[-\frac{1}{2}(\mathbf{R} - \mathbf{R}_a)^{\mathrm{T}}\mathbf{S}_a^{-1}(\mathbf{R} - \mathbf{R}_a)\right], \tag{10}$$

where $\mathbf{S}_a$ is the error covariance matrix associated with the a priori guess. Given the symmetry of the Gaussian distribution, the ''best'' estimate of a rainfall profile from Eq. (7) is that which maximizes the joint probability

$$P[\mathbf{Z} \mid F(\mathbf{R})]P_a(\mathbf{R} \mid \mathbf{R}_a) \propto \exp\left\langle -\frac{1}{2}\{[F(\mathbf{R}) - \mathbf{Z}]^{\mathrm{T}}\mathbf{S}_Z^{-1}[F(\mathbf{R}) - \mathbf{Z}] + (\mathbf{R} - \mathbf{R}_a)^{\mathrm{T}}\mathbf{S}_a^{-1}(\mathbf{R} - \mathbf{R}_a)\}\right\rangle \tag{11}$$

or, alternatively, minimizes the scalar cost function

$$\Phi(\mathbf{R}, \mathbf{R}_a, \mathbf{Z}) = [F(\mathbf{R}) - \mathbf{Z}]^{\mathrm{T}}\mathbf{S}_Z^{-1}[F(\mathbf{R}) - \mathbf{Z}] + (\mathbf{R} - \mathbf{R}_a)^{\mathrm{T}}\mathbf{S}_a^{-1}(\mathbf{R} - \mathbf{R}_a), \tag{12}$$

with respect to the rain-rate profile $\mathbf{R}$. The resulting rain-rate profile is

$$\hat{\mathbf{R}} = \mathbf{R}_a + \mathbf{S}_a\mathbf{K}^{\mathrm{T}}\mathbf{S}_Z^{-1}[\mathbf{Z} - F(\hat{\mathbf{R}})]. \tag{13}$$

Here $\mathbf{K} = \partial F/\partial \mathbf{R}$ is the Kernel or weighting function representing the sensitivity of the model to the parameter being retrieved. From Eq. (13) it is clear that a model that is very sensitive to the rainfall-rate profile is desirable since the Kernel functions weight the measurement portion of the retrieval. It is worth noting that, under the present assumptions of uncorrelated, unbiased, Gaussian error statistics, the maximum-likelihood estimate computed here is identical to the minimum variance solution (Daley 1991), which guarantees that $\mathbf{R}$ estimated using Eq. (13) will be the best possible fit to the observations given our uncertainty estimates.

Equation (13) is implemented numerically through a Newtonian iteration scheme,

$$\hat{\mathbf{R}}_{i+1} - \hat{\mathbf{R}}_i = \mathbf{S}_{\hat{R}}\{\mathbf{K}_i^T\mathbf{S}_Z^{-1}[\mathbf{Z} - F(\hat{\mathbf{R}}_i)] + \mathbf{S}_a^{-1}(\mathbf{R}_a - \hat{\mathbf{R}}_i)\}, \quad (14)$$

where $\mathbf{S}_{\hat{R}} = (\mathbf{S}_a^{-1} + \mathbf{K}_i^T\mathbf{S}_Z^{-1}\mathbf{K}_i)^{-1}$ is the covariance matrix of the retrieved rainfall profile. The iteration proceeds until such time as the covariance-weighted square difference between successive estimates is much less than the total number of independent variables being retrieved, in this case the number of layers in the atmosphere, N_l:

$$(\hat{\mathbf{R}}_{i+1} - \hat{\mathbf{R}}_i)^T\mathbf{S}_{\hat{R}}^{-1}(\hat{\mathbf{R}}_{i+1} - \hat{\mathbf{R}}_i) \ll N_l. \quad (15)$$

b. Error diagnostics

The preceding optimal estimation formulation of the inversion problem furnishes a number of useful diagnostics to measure the quality of the results. The most important of these is the covariance matrix of the retrieved parameters:

$$\mathbf{S}_{\hat{R}} = (\mathbf{S}_a^{-1} + \mathbf{K}_i^T\mathbf{S}_Z^{-1}\mathbf{K}_i)^{-1}. \quad (16)$$

Equation (16) provides a direct estimate of the uncertainty in the retrieved rain-rate profile due to uncertainties associated with the a priori profile, forward model, and measurements themselves. The diagonal elements of $\mathbf{S}_{\hat{R}}$ are the variances in the retrieved rain rate at each level while the off-diagonal elements indicate correlations between uncertainties at different levels. In regard to the details of the forward model F, for example, uncertainties in the parameter vector $\mathbf{b}$, such as those associated with assumptions regarding the highly variable DSD, must be accounted for in the measurement and model covariance matrix $\mathbf{S}_Z$. An appropriate $\mathbf{S}_Z$ dictates the reliability of the observations and forward model in the retrieval and ensures a reliable estimate of retrieval accuracy through Eq. (16).

Defining the matrix

$$\mathbf{A} = \mathbf{S}_{\hat{R}}\mathbf{K}_i^T\mathbf{S}_Z^{-1}\mathbf{K}_i, \quad (17)$$

Eq. (14) can be written,

$$\hat{\mathbf{R}}_{i+1} - \hat{\mathbf{R}}_i = \mathbf{A}\mathbf{K}_i^{-1}[\mathbf{Z} - F(\hat{\mathbf{R}}_i)] + (\mathbf{I} - \mathbf{A})(\mathbf{R}_a - \hat{\mathbf{R}}_i). \quad (18)$$

In this way, the contributions to the retrieved profile from the measurements and from the a priori profile are isolated. In an ideal retrieval, the so-called a priori matrix $\mathbf{A}$ will be an identity indicating that the retrieval is based exclusively on the measurements. Departures from the identity represent a combination of influences from the a priori data and reflectivity measurements from different atmospheric levels on the rain rate retrieved at a given level.

One can investigate the validity of the assumption of Gaussian error statistics using the χ^2 test. If the assumption is valid,

$$\chi^2 = [F(\hat{\mathbf{R}}) - \mathbf{Z}]^T\mathbf{S}_Z^{-1}[F(\hat{\mathbf{R}}) - \mathbf{Z}] + (\hat{\mathbf{R}} - \mathbf{R}_a)^T\mathbf{S}_a^{-1}(\hat{\mathbf{R}} - \mathbf{R}_a) \quad (19)$$

will be approximately equal to the number of independent parameters in the retrieval, in this case N_l. In cases where our physical assumptions, particularly those relating to the DSD, are grossly different from those being observed or in the event that the Gaussian distribution and assumed variances do not properly characterize uncertainties in the measurements and model, χ^2 will be much greater than N_l. In global applications, a significant number of retrievals characterized by large χ^2 is indicative of overoptimistic error covariance assumptions in the algorithm, such as a misrepresentation of the DSD variability encountered by the satellite. On the other hand, if χ^2 is much less than N_l, the measurement, model, and/or a priori covariances may have been overestimated and $\mathbf{S}_{\hat{R}}$ will correspondingly overestimate the retrieval uncertainty.

TABLE 1. The Z–R and k–R parameters used to initialize rainfall retrieval. The distinction between the ''high'' and ''low'' fits occurs at 17.8 mm h^{-1} at 14 GHz and 11.0 mm h^{-1} at 94 GHz.

Parameter	14 GHz (low)	14 GHz (high)	94 GHz (low)	94 GHz (high)
a	155.1	243.4	29.2	42.2
b	1.61	1.45	0.71	0.55
α	0.014	0.020	0.68	0.88
β	1.23	1.10	0.78	0.67

c. Algorithm initialization

There is generally no ''average'' climatological profile of rainfall available to use as an a priori guess. As a result, we resort to the more traditional relationships

$$Z = aR^b \quad \text{and} \quad k_{\text{ext}} = \alpha R^\beta \quad (20)$$

to obtain $\mathbf{R}_a$, and this rainfall profile is used to initialize the iteration. Table 1 summarizes parameters determined assuming an MP size distribution of spherical raindrops and Mie theory for the backscatter cross-sections at 14 and 94 GHz. Because of the departure from the linear relationship as Mie effects become important, the fit was divided into two regions to improve results.

To summarize, the retrieval proceeds as follows:

- Infer an initial rain rate and extinction coefficient for the uppermost rain layer using the appropriate Z–R and k–R relations.
- Correct the measured reflectivity in the next layer for the attenuation due to the one above it and determine an initial rain rate and extinction coefficient for that layer.
- Repeat for all layers, correcting the measured reflec-

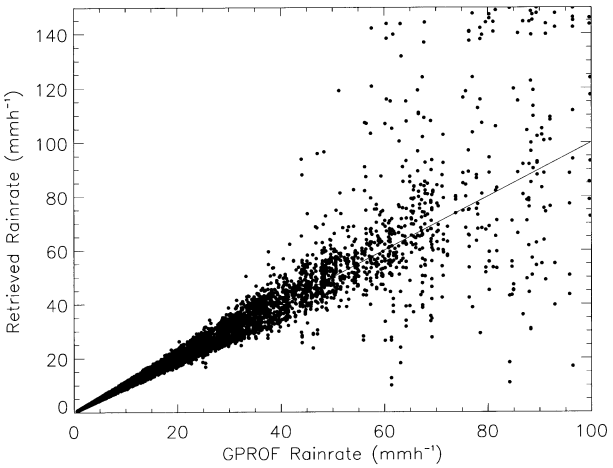

FIG. 2. Scatterplot of retrieved near-surface rainfall against the GPROF input at 14 GHz.

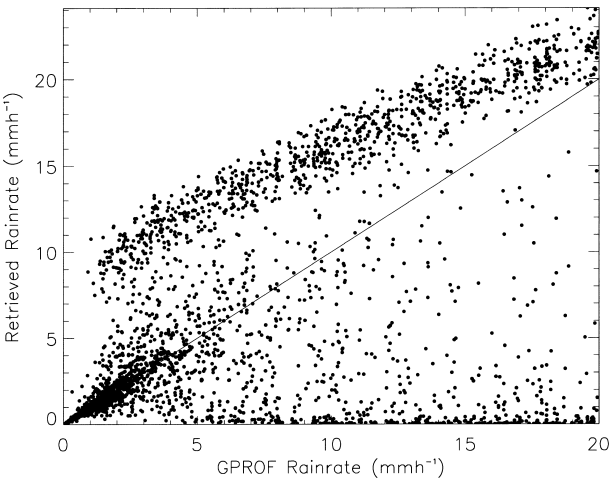

FIG. 3. As in Fig. 2, but for retrievals at 94 GHz.

tivity of each layer for the attenuation due to all layers above it.
- Using this initial profile of rain rate, simulate reflectivities using the radar forward model [Eq. (5)].
- Compute a new rain-rate profile using Eq. (14).
- Iterate until Eq. (15) is satisfied.

4. Synthetic retrievals

The algorithm was tested using the cloud database used in the Goddard Profiling Algorithm (GPROF), which is currently employed in rainfall retrievals from the TRMM Microwave Imager [see Kummerow and Giglio (1994) and Olson et al. (1996) for details regarding the cloud database and the GPROF algorithm]. The database consists of approximately 10 000 cloud and rainfall profiles varying from nonprecipitating cirrus and stratus clouds to heavily precipitating cumulonimbus cloud complexes and represents a wide range of conditions with which to test the algorithm. In order to illustrate the utility of the model, reflectivity profiles with 0.5-km vertical resolution were computed for all cloud and rain-rate profiles in the database assuming an MP distribution of spherical raindrops and cloud droplets of diameter D, $N(D) = N_0 e^{-\Lambda D}$. The distribution is entirely described by the rain rate R assuming the parameters $N_0 = 8 \times 10^6\ \mathrm{m}^{-4}$ and $\Lambda = 4.100R^{-0.21}\ \mathrm{mm}^{-1}$. These reflectivity profiles were then perturbed by adding a randomly distributed noise component and run through the retrieval algorithm to recover the original profile. The noise was set to 1 dB (or 23%) for profiles with surface rain rates less than 20 mm h^{-1} and 2 dB (or 46%) for higher rain rates to reflect the fact that errors due to particle shape are more significant for larger raindrops than smaller ones (Green 1975). In the retrieval, the measurement covariance matrix is assumed to be diagonal with elements equal to 1.0 dB^2 (or 4.0, where applicable). No attempt is made at this time to account for uncertainties in DSD parameters introduced by their variability in nature but it is acknowledged that this contribution will be extremely important in operational applications using this technique. A variance of 25.0 $\mathrm{mm}^2\ \mathrm{h}^{-2}$ is assumed in all a priori rain rates and all correlations between errors at different levels are neglected. In this way, the retrieval is based far more heavily on the measurements and the a priori merely serves as an initial guess and an extremely weak positivity constraint on the retrieval. In addition, the assumption of high a priori variances minimizes errors incurred as a result of neglecting correlations between uncertainties at different levels, which are, in practice, extremely difficult to determine.

A scatterplot of retrieved surface rain rate against the GPROF input at 14 GHz is presented in Fig. 2. The results show excellent agreement for surface rain rates below 40 mm h^{-1}. Significant attenuation by large raindrops at higher rain rates, however, degrades the quality of the retrievals. Figure 3 shows similar results obtained from a retrieval using reflectivities at 94 GHz. Attenuation is severe for all rainfall at 94 GHz and only rain rates less than 1.5 mm h^{-1} are retrieved accurately in the absence of additional information.

Figures 4 and 5 present the estimated error in the retrieved surface rainfall rate and the corresponding component of the a priori matrix at 14 GHz. Together, the two figures demonstrate that, under the present assumptions, the uncertainty in retrieved rainfall is below 30% for all profiles with surface rain rates between 0 and 40 mm h^{-1}. In heavier rain, the retrieval relies heavily on the a priori guess, so, although the retrieval errors appear to be acceptable, the results do not reflect the information contained in the measurements and must be discarded.

At 94 GHz, the enormous retrieval uncertainties illustrated in Fig. 6 demonstrate the fact that reflectivity measurements do not provide sufficient information to

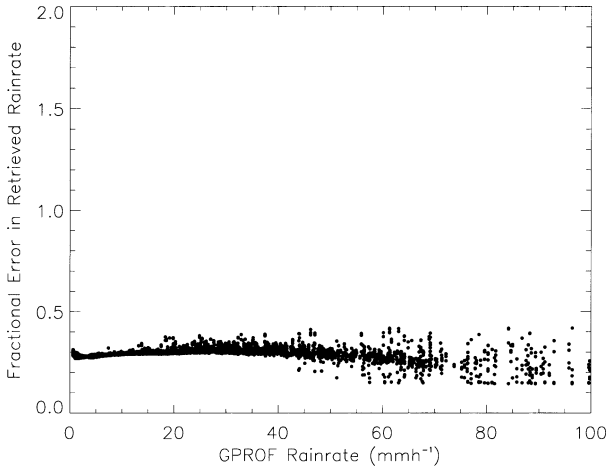

FIG. 4. Error in retrieved rain rate as a function of GPROF rain rate for the 14-GHz synthetic retrievals.

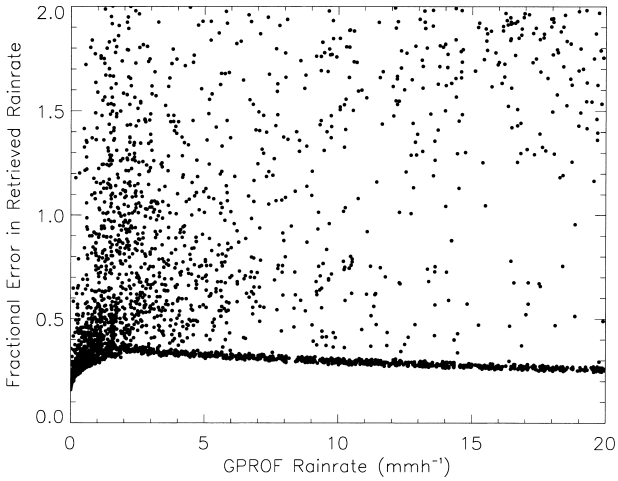

FIG. 6. As in Fig. 4, but at 94 GHz.

accurately determine surface rainfall rate. The fractional error only remains within tolerable limits up to about 1.0 mm h^{-1}. In heavier rain, uncertainties become large and differences in the vertical distribution of rainfall above the surface give rise to scatter in the results. Many of the 94-GHz retrievals also yield extremely high values of χ^2 (not shown) indicating that the retrieved profile of rainfall seldom attains satisfactory agreement with the observations.

These results may be attributed to the method adopted for applying the attenuation correction. Since the procedure, which is analogous to the Hitschfeld and Borden (1954) method, first corrects the layers closest to the radar and then adjusts lower layers according to rain rates derived from these corrections, it leads to the propagation and magnification of errors as the algorithm proceeds to lower levels within the cloud. Figure 7, which presents retrieved rain rates at 4.0 km, near the top of the liquid rain column, supports this hypothesis. Although the retrievals exhibit some deviation from the input at high rain rate, the agreement is clearly far superior than that at the surface. Figure 8 shows that uncertainties in retrieved rain rates are better constrained at 4.0 km.

5. Precipitation water path as a constraint

Because of the severity of attenuation by rainfall at high frequencies, it is not sufficient to rely exclusively on a profile of radar reflectivity to make estimates of rainfall profiles. Fortunately, many spaceborne platforms such as TRMM, offer additional sources of information from other instruments. Microwave radiometers can be used to obtain an estimate of the total precipitation water path [PWP; see, e.g., Fujita et al. (1985); Alishouse et al. (1990)], which is defined as the column-integrated liquid water that is in the form of precipitation. This estimate complements the radar re-

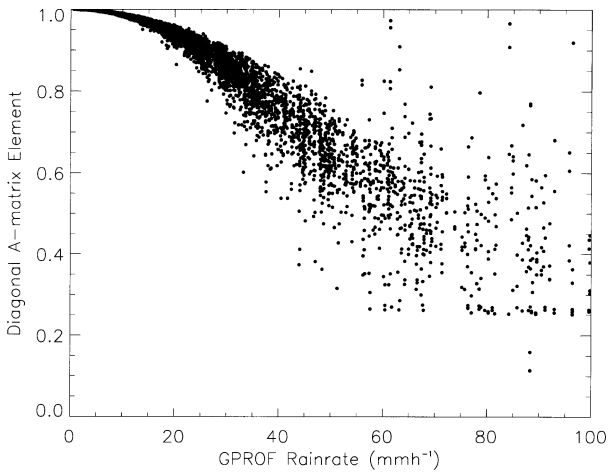

FIG. 5. Diagonal element of the a priori matrix corresponding to the surface rain-rate bin as a function of rain rate for the GPROF 14-GHz retrievals.

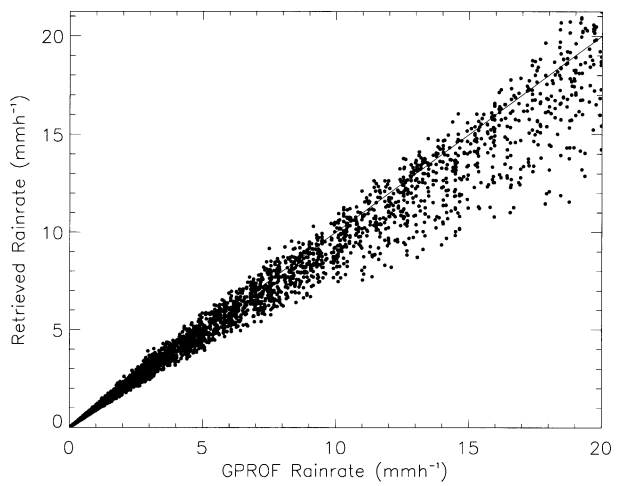

FIG. 7. As in Fig. 3, but at an altitude of 4.0 km.

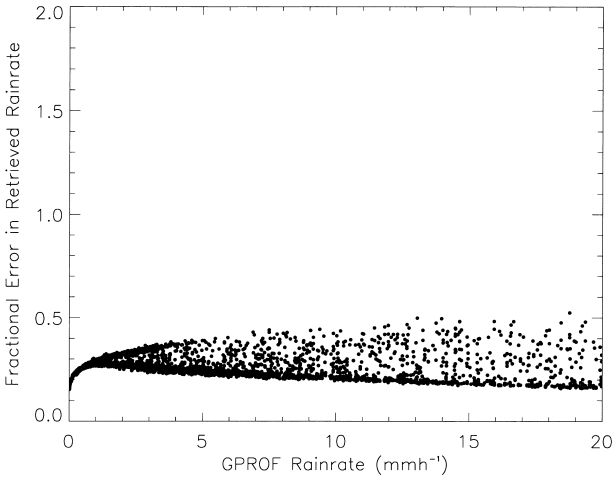

FIG. 8. As in Fig. 6, but at an altitude of 4.0 km.

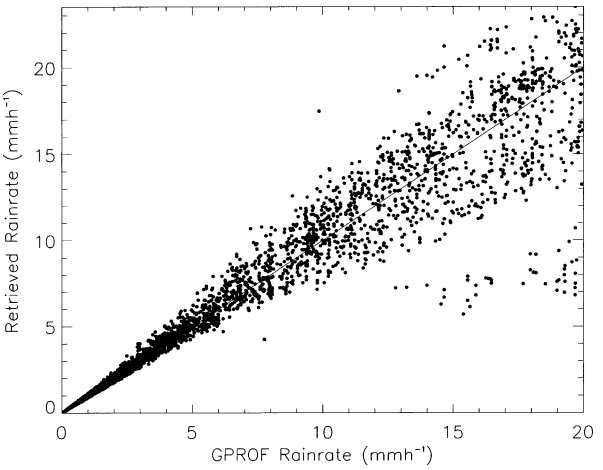

FIG. 9. Scatterplot of retrieved near-surface rainfall rate against the GPROF input at 14 GHz with a precipitation water path constraint.

flectivity measurements in that it imposes a constraint on the total attenuation through the rain column.

a. Theory

In the presence of such a constraint, the cost function can be expressed as

$$\Phi(\mathbf{R}, \mathbf{R}_a, \mathbf{Z}) = [F(\mathbf{R}) - \mathbf{Z}]^{\mathrm{T}}\mathbf{S}_R^{-1}[F(\mathbf{R}) - \mathbf{Z}] + (\mathbf{R} - \mathbf{R}_a)^{\mathrm{T}}\mathbf{S}_a^{-1}(\mathbf{R} - \mathbf{R}_a) + \frac{(\mathrm{PWP}_{\mathrm{sim}} - \mathrm{PWP}_{\mathrm{obs}})^2}{\sigma_{\mathrm{PWP}}^2}, \quad (21)$$

where $\mathrm{PWP}_{\mathrm{obs}}$ is the observed PWP with standard deviation σ_{PWP}, and $\mathrm{PWP}_{\mathrm{sim}}$ is the liquid water path obtained by integrating the rain-rate profile in height. Minimizing with respect to $\mathbf{R}$, we obtain

$$\hat{\mathbf{R}}_{i+1} = \mathbf{S}_{\hat{R}}\left\{\mathbf{S}_a^{-1}\mathbf{R}_a + \mathbf{K}_i^{\mathrm{T}}\mathbf{S}_Z^{-1}[\mathbf{Z} - F(\hat{\mathbf{R}}_i)] + \frac{1}{\sigma_{\mathrm{PWP}}^2}\mathbf{L}_i\Delta z(\mathrm{PWP}_{\mathrm{obs}} - \mathrm{PWP}_{\mathrm{sim}} + \mathbf{L}_i^{\mathrm{T}}\Delta z\hat{\mathbf{R}}_i)\right\}, \quad (22)$$

with $\mathbf{S}_{\hat{R}} = (\mathbf{S}_a^{-1} + \mathbf{K}_i^{\mathrm{T}}\mathbf{S}_Z^{-1}\mathbf{K}_i + (\Delta z^2/\sigma_{\mathrm{PWP}}^2)\mathbf{L}_i\mathbf{L}_i^{\mathrm{T}})^{-1}$. The vector $\Delta z\mathbf{L}$ consists of the derivatives of PWP with respect to the rain rate at each level.

One measure of the strength of the constraint is to determine the relative contributions of the measurements, a priori guess, and the constraint to the retrieval error covariance matrix $\mathbf{S}_{\hat{R}}$. Defining

$$\mathbf{D}_Z = \mathbf{S}_{\hat{R}}\mathbf{K}^{\mathrm{T}}\mathbf{S}_Z^{-1}, \quad (23a)$$

$$\mathbf{D}_a = \mathbf{S}_{\hat{R}}\mathbf{S}_a^{-1}, \quad \text{and} \quad (23b)$$

$$\mathbf{D}_{\mathrm{PWP}} = \frac{\mathbf{S}_{\hat{R}}\mathbf{L}\Delta z}{\sigma_{\mathrm{PWP}}^2}, \quad (23c)$$

the total retrieval error covariance matrix can be expressed as

$$\mathbf{S}_{\hat{R}} = \mathbf{D}_Z\mathbf{S}_Z\mathbf{D}_Z^{\mathrm{T}} + \mathbf{D}_a\mathbf{S}_a\mathbf{D}_a^{\mathrm{T}} + \mathbf{D}_{\mathrm{PWP}}\mathbf{S}_{\mathrm{PWP}}\mathbf{D}_{\mathrm{PWP}}^{\mathrm{T}}, \quad (24)$$

where $\mathbf{S}_{\mathrm{PWP}}$ is a diagonal matrix with σ_{PWP}^2 on the diagonal. Diagonal elements of each term represent the contributions of the measurements, a priori guess, and the constraint to the retrieval uncertainty making it possible to assess the relative strengths of the three components in determining the rain-rate profile. In addition, the χ^2 test can, again, be employed to test the assumption of Gaussian statistics and the values assumed for the variances:

$$\chi^2 = [F(\hat{\mathbf{R}}) - \mathbf{Z}]^{\mathrm{T}}\mathbf{S}_Z^{-1}[F(\hat{\mathbf{R}}) - \mathbf{Z}] + (\hat{\mathbf{R}} - \mathbf{R}_a)^{\mathrm{T}}\mathbf{S}_a^{-1}(\hat{\mathbf{R}} - \mathbf{R}_a) + \frac{(\mathrm{PWP}_{\mathrm{obs}} - \mathrm{PWP}_{\mathrm{sim}})^2}{\sigma_{\mathrm{PWP}}^2} \approx N_l. \quad (25)$$

b. Results

Surface rain-rate retrievals at 94 GHz with a precipitation water path constraint are presented in Fig. 9. The constraint variance was taken to be 10% and no other retrieval parameters were changed. An accurate estimate of PWP forces the algorithm to put the correct water mass in the atmosphere while the radar reflectivities determine how this mass is distributed in the vertical. This emphasizes the compatibility of active and passive microwave data in rainfall retrievals. The value of an accurate PWP estimate is further evidenced by Tables 2 and 3, which compare the correlation coefficients and their standard deviations for unconstrained and constrained retrievals at 14 and 94 GHz, respectively. The constraint reduces the retrieval standard deviation in all rain-rate bins at both frequencies. At 14 GHz, errors are reduced by between 20% and 30% over the entire range

TABLE 2. Correlation coefficients and std dev (mm h^{-1}) for unconstrained and constrained synthetic surface rain-rate retrievals at 14 GHz.

	Unconstrained		Constrained (σ_{PWP} = 10%)	
Rain-rate range	Correlation	Std dev	Correlation	Std dev
0–20 mm h^{-1}	0.991	0.834	0.993	0.739
20–40 mm h^{-1}	0.869	3.267	0.918	2.434
40–60 mm h^{-1}	0.521	9.989	0.604	7.646
60–80 mm h^{-1}	0.305	24.407	0.394	16.500
80–100 mm h^{-1}	0.166	37.805	0.063	31.366
0–100 mm h^{-1}	0.932	8.375	0.958	6.346

of rain rates tested, and rain rates up to 80 mm h^{-1} exhibit standard deviations of less than 25% when constrained. At 94 GHz, standard deviations in the absence of a constraint are on the order of 50% over the range of rain rates presented but are reduced by a factor of 5 when it is introduced. Biases introduced by attenuation affects are also substantially reduced when the PWP constraint is enforced.

Figure 10 shows retrievals of selected rainfall profiles from the GPROF database at the frequency of the TRMM PR with constraints of varying strength. The constraint has little impact on the PR retrievals below 30 mm h^{-1} regardless of its accuracy. At a near-surface rain rate of over 45 mm h^{-1}, however, the surface rain rate is underestimated by 25% in the absence of a constraint but improves significantly with a strong one. In extremely heavy rain, where attenuation effects are severe, an accurate PWP estimate improves retrieved surface rain-rate errors from 40% to less than 10%. Similar results are presented in Fig. 11 for the CloudSat CPR. Because of the different range of rainfall rates detectable by the CPR, the two heaviest rain profiles have been replaced by light rain cases in this figure. In extremely light rain, the retrieved rainfall profile varies little with the addition of a constraint. For all other rainfall, the constraint has a marked impact. Note that the accuracy in the PWP estimate required to obtain an accurate retrieval increases with rain rate following the increasing trend exhibited by the attenuation.

Figures 10 and 11 also illustrate a very important, yet heretofore overlooked, benefit to using coincident cloud and precipitation radar measurements. The 14-GHz radar cannot detect rainfall lighter than 0.7 mm h^{-1} as is evidenced by the upper-left plot in Fig. 10. The cloud radar, on the other hand, is perfectly suited to retrieve light rain as well as cloud but is incapable of quantitatively measuring heavy rainfall. Despite their low rainfall rates, light rain systems typically occur over large areas and are long-lived relative to heavy rain. They may, therefore, account for a significant fraction of the total precipitation globally and cannot be ignored when studying the impacts of the hydrological cycle on the earth's climate system. In addition, given the radiative impact of clouds in driving global circulations (see Stephens et al. 2000, and references therein, manuscript submitted to *Bull. Amer. Meteor. Soc.*), they represent a significant omission from the information provided by a lower-frequency radar. The synergy offered by these two instruments makes them well-suited to be operated simultaneously in future studies.

Contributions from the measurements, a priori guess, and constraint to the overall retrieval uncertainty at 94 GHz are illustrated in Fig. 12 for a moderate (σ_{PWP} = 10%) constraint. In the absence of attenuation in extremely light rain, the retrieval is dominated by the reflectivity measurements. In each of the other cases, the retrieval is dominated by measurements at upper levels and by the constraint at lower levels. Once again this supports the hypothesis that the constraint adds important attenuation information to the algorithm. Last, it is somewhat disturbing to note that the algorithm relies heavily on the a priori guess in the highest rainfall shown. Given the concerns raised earlier as to the accuracy of the initial guess, this serves as a warning to restrict application of this algorithm to rain rates of 10 mm h^{-1} or less when using the high-frequency radar unless an extremely accurate PWP estimate is available. This figure also highlights the powerful uncertainty

TABLE 3. As in Table 2, but for retrievals at 94 GHz.

	Unconstrained		Constrained (σ_{PWP} = 10%)	
Rain-rate range	Correlation	Std dev	Correlation	Std dev
0–5 mm h^{-1}	0.718	2.050	0.992	0.170
5–10 mm h^{-1}	0.153	5.578	0.837	1.046
10–15 mm h^{-1}	0.126	7.538	0.547	1.923
15–20 mm h^{-1}	0.105	9.774	0.245	3.530
0–20 mm h^{-1}	0.651	5.184	0.968	1.477

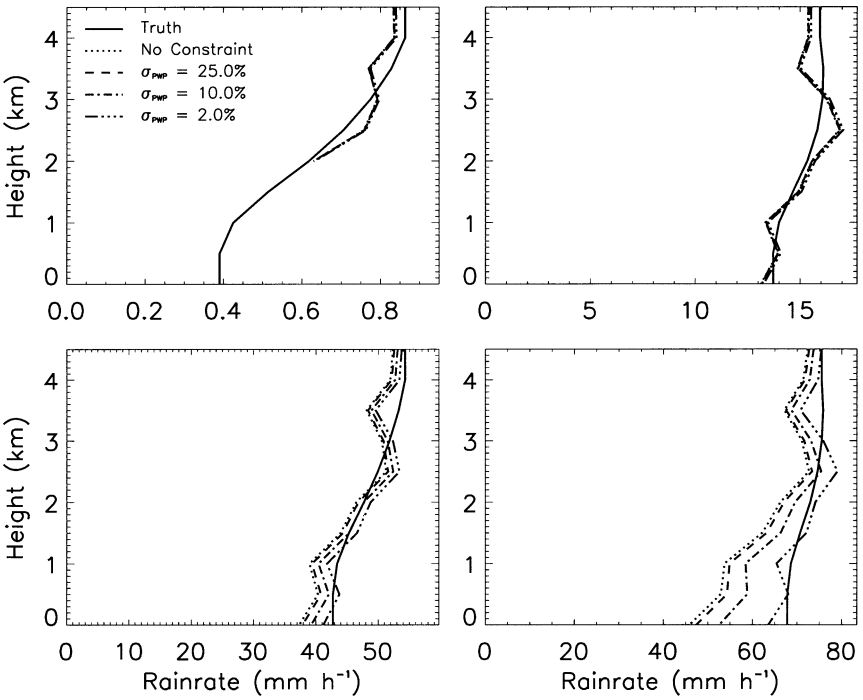

FIG. 10. Sample rainfall retrievals at 14 GHz with constraints of varying strength against truth for near-surface rain rates of (top left) near 0.8, (top right) 15.0, (bottom left) 50.0, and (bottom right) 80.0 mm h^{-1}.

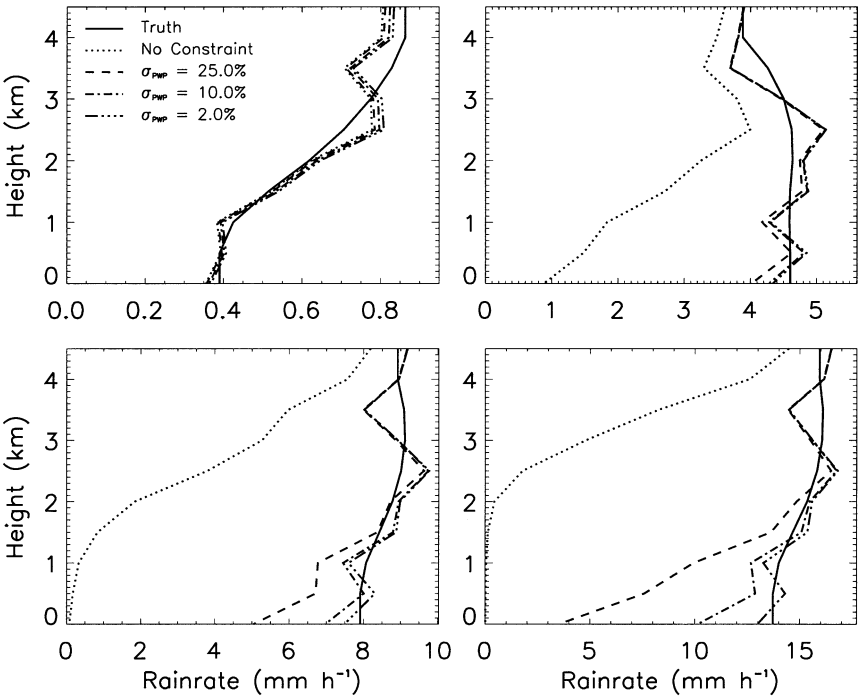

FIG. 11. As in Fig. 10, but for retrievals of lighter rain at 94 GHz for near-surface rain rates of (top left) near 0.8, (top right) 4.5, (bottom left) 8.0, and (bottom right) 15.0.

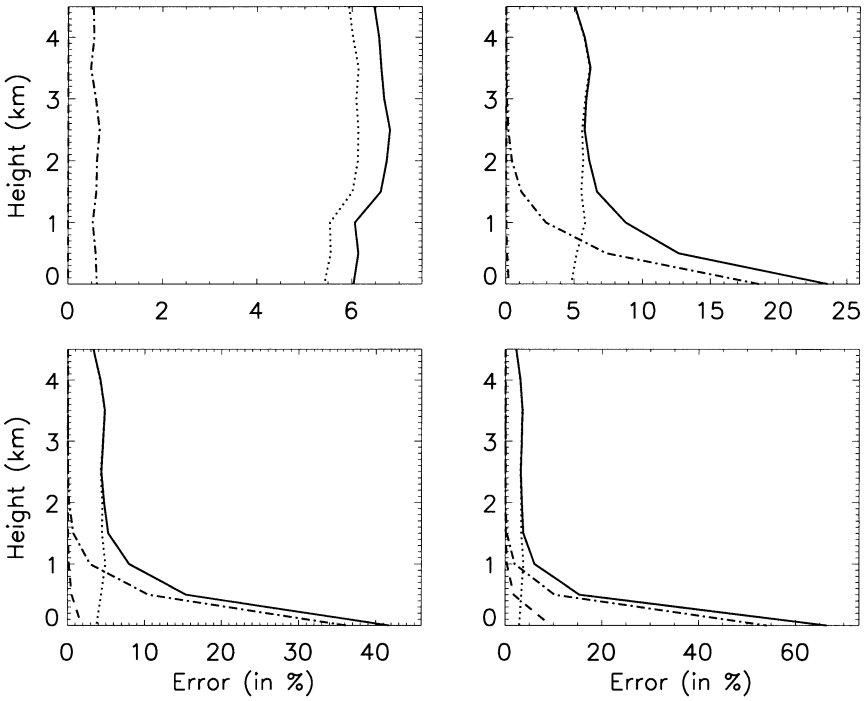

FIG. 12. The measurement (dotted line), a priori (dashed line), and PWP constraint (dot–dashed line) contributions to the total error (solid line) in the retrievals from Fig. 11, assuming a constraint accuracy of 10%. Rainfall rates are as in Fig. 11.

analyses that are possible within the constructs of an optimal estimation-based retrieval. In addition to obtaining a rainfall estimate and an associated uncertainty, the dominant information driving the retrieval is demonstrated.

The ratio of the constraint contribution to the 94-GHz retrieval uncertainty to those of the a priori guess and measurements is displayed in Fig. 13 as a function of constraint accuracy. The peak in these curves can be taken as an optimal σ_{PWP} for the retrieval. If the constraint is significantly less accurate, its impact on the retrieval will be minimal while the benefits of increasing its accuracy beyond the peak are not likely to be significant enough to warrant the extra effort required to obtain such accuracy. From the magnitudes of the peaks it is clear that the constraint has little impact on the retrieval in extremely light rain but very significant, and comparable, impact for the three remaining rain profiles. It is also apparent that the optimal constraint accuracy increases with increasing rain rate and with decreasing altitude. The greater the attenuation, the more accurate the PWP estimate must be to correct for it. Depending on the specific goals for the application of the algorithm, an estimate of PWP with only moderate accuracy might be all that is required to constrain the retrieval. In applications involving the use of a high-frequency radar to supplement rainfall information obtained at lower frequency, for example, retrievals in rainfall lighter than 4 or 5 mm h^{-1} may be of primary importance, in which case a PWP estimate accurate to 20% is sufficient.

Figure 14 illustrates the physics introduced in the retrieval process from both the active and passive measurements. Shown are rain-rate profiles at each step of the iteration process for a single retrieval from the database with constraints at four different accuracies. The upper-left plot illustrates the propagation of errors due to attenuation in the absence of a constraint. In this case, the algorithm suffers from the inability to distinguish between unattenuated light rain and attenuated heavier rain, retrieving the former when, in fact, viewing the latter. A modest PWP constraint ($\sigma_{\text{PWP}} = 25\%$) results in significantly improved agreement with the true profile, particularly above 1.5 km. When stricter constraints are imposed, as in the lower two plots, the algorithm increases the rain rate at all levels in subsequent iterations, eventually attaining good agreement with the true profile. Note that in every case the same initial guess, based on the *Z–R* and *k–R* relations, is made. The presence of a PWP constraint, however, forces the algorithm to ''pump'' more water into the column in the three cases involving a constraint. The constraint, therefore, determines the PWP in the atmospheric column during the first few iterations and the reflectivity measurements establish its vertical distribution in the remaining iterations. By virtue of Eqs. (15) and (22), the process cannot stop until agreement is obtained with both measurements.

It must be noted that the fact that the same assumptions are made in both the forward and inverse models undoubtedly masks the impact of variable DSD and par-

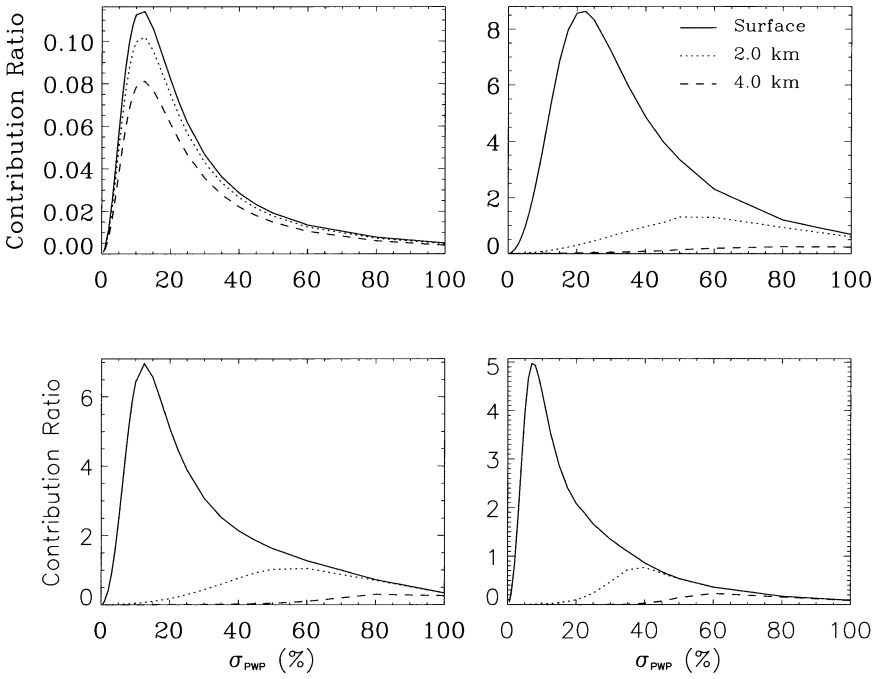

FIG. 13. Ratio of the constraint contribution to the total error to the sum of the corresponding measurement and a priori contributions as a function of constraint strength for three heights for the rainfall retrievals in Fig. 11. Rainfall rates are as in Fig. 11.

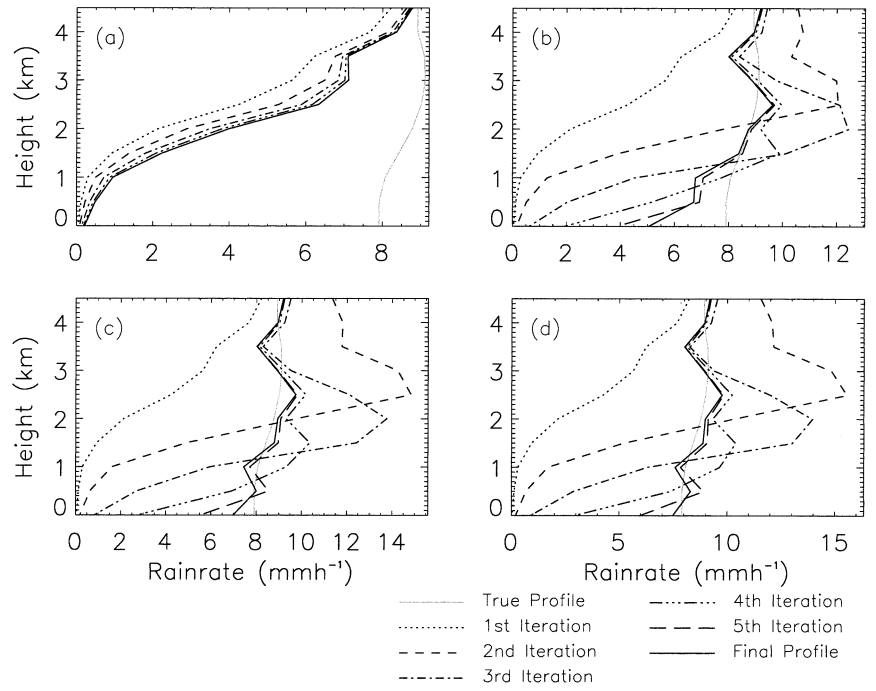

FIG. 14. Iterations in a synthetic retrieval at 94 GHz with (a) no constraint, (b) a constraint with $\sigma_{PWP} = 25.0$, (c) a constraint with $\sigma_{PWP} = 10.0$, and (d) a constraint with $\sigma_{PWP} = 2.0$.

ticle shape on the results but synthetic retrievals of this type are not necessarily meant to provide a rigorous test of the algorithm. This study demonstrates the feasibility of applying this type of algorithm at attenuating frequencies. In the future, studies employing airborne and spaceborne radar data with ground validation will be used. In such studies the DSD and shape of the raindrops can be modified to give the best overall fit to all data available including passive microwave radiances.

6. Conclusions

With the growing trend toward space-based observation platforms that carry high-frequency cloud and rain profiling radars, the need for accurate, flexible algorithms for retrieving rainfall at attenuating frequencies is paramount. In this paper, we have presented an algorithm that is not, in principle, restricted by assumptions of size distribution or particle shape and accounts for attenuation through direct integration of two-way extinction due to all rain along the path to each target layer. The algorithm maximizes a posterior probability density function derived from an assumption of uncorrelated, unbiased errors following a Gaussian distribution. The Gaussian distribution, by virtue of its symmetry, adds the least bias of any assumed error distribution in the absence of additional information and ensures equivalence between the location of its maximum and its mean, a necessary condition for the solution to be optimal.

Preliminary results, using simplifying assumptions, illustrate the utility of the algorithm, particularly at low frequencies. At 14 GHz, synthetic retrievals of rainfall profiles using the GPROF cloud database accurately reproduce the input for rain rates as high as 40 mm h^{-1}. At 94 GHz, however, the algorithm grossly over- or underestimates surface rainfall at all rain rates above 1.5 mm h^{-1} because of instability inherent in the method employed to correct for attenuation. The PIA approach to correct for attenuation, which makes use of the surface-return echo to estimate the total attenuation through the rain column, is stable and yields much more accurate results when attenuation is severe (Iguchi and Meneghini 1994). This is confirmed by the remarkable improvement in the retrieval when a precipitation water path constraint is imposed on the retrieval. Since the PIA derives from the precipitation water path, both constraints perform essentially the same function. Either method (or both) can be used in the present algorithm with very little modification. It is also worth noting that the application of this algorithm to the CloudSat radar is explicitly for the purpose of retrieving very light rain that may not be detectable at lower frequencies. In this light, the results presented here are encouraging.

While the assumption of an exponential DSD and spherical particles oversimplifies the problem, the early results presented above suggest that it is worth pursuing extensions of the model to include more direct estimation of size distribution parameters making more complete use of the other observations available to both the TRMM and CloudSat missions. In a slightly more general form, Eq. (12) can be written as

$$\Phi(\mathbf{x}, \mathbf{x}_a, \mathbf{y}) = [F(\mathbf{x}) - \mathbf{y}]^{\mathrm{T}}\mathbf{S}_y^{-1}[F(\mathbf{x}) - \mathbf{y}] + (\mathbf{x} - \mathbf{x}_a)^{\mathrm{T}}\mathbf{S}_a^{-1}(\mathbf{x} - \mathbf{x}_a), \quad (26)$$

where $\mathbf{x}$ is a more general vector of retrieval parameters, perhaps consisting of DSD parameters at each level, $\mathbf{y}$ is a general vector of satellite-based measurements, and F is an appropriate combination of forward models that map the retrieval parameters into the basis of these measurements. This equation can be solved in exactly the same manner as above, yielding an iterative solution to determine the best estimate of rain rate based on all available observations simultaneously. As the TRMM PR algorithms have demonstrated, directly accounting for DSD variability is of paramount importance for the next generation of satellite radar retrievals. Studies are currently under way to recast the algorithm in terms of a more general DSD and a parallel effort is being undertaken to directly incorporate radiances from the TMI to provide the more rigorous constraint required to estimate a more flexible DSD.

In the near future, the CloudSat CPR in formation with the Advanced Microwave Scanning Radiometer (AMSR-E) on board the Earth Observing System (EOS) Aqua satellite will provide an unprecedented opportunity to examine the possibility of making quantitative rainfall estimates from a combination of a microwave radiometer and a 94-GHz cloud radar in space. The algorithm presented here is ideally suited for this purpose.

Acknowledgments. The authors thank Dr. Chris Kummerow and his research group at Colorado State University for their support in the acquisition of the Goddard Profiling Algorithm cloud databases. We also thank Drs. Richard Engelen and Richard Austin for numerous enlightening discussions throughout the development of this algorithm. This research was funded through NASA TRMM Research Grant NAG5-7719.

REFERENCES

Alishouse, J. C., S. A. Snyder, J. Vongsathorn, and R. R. Ferraro, 1990: Determination of oceanic total precipitable water from the SSM/I. *IEEE Trans. Geosci. Remote Sens.,* **28,** 811–816.

Amayenc, P., J. P. Diguet, M. Marzoug, and T. Tani, 1996: A class of single- and dual-frequency algorithms for rain-rate profiling from a spaceborne radar. Part II: Tests from airborne radar measurements. *J. Atmos. Oceanic Technol.,* **13,** 142–164.

Cess, R. D., and Coauthors, 1993: Uncertainties in carbon dioxide radiative forcing in atmospheric general circulation models. *Science,* **262,** 1252–1255.

Daley, R., 1991: *Atmospheric Data Analysis.* Cambridge University Press, 471 pp.

Engelen, R. J., and G. L. Stephens, 1999: Characterization of water vapour retrievals from TOVS/HIRS and SSM/T-2 measurements. *Quart. J. Roy. Meteor. Soc.,* **125,** 331–351.

Fujita, M., and M. Satake, 1997: Rainfall rate profiling with attenuating-frequency radar using nonlinear LMS technique under a constraint on path-integrated rainfall rate. *Int. J. Remote Sens.,* **18,** 1137–1147.

——, K. Okamoto, H. Masuko, T. Ojima, and N. Fugono, 1985: Quantitative measurements of path-integrated rain rate by an airborne microwave radiometer over the ocean. *J. Atmos. Oceanic Technol.,* **2,** 285–292.

Green, A. W., 1975: An approximation for the shapes of large raindrops. *J. Appl. Meteor.,* **14,** 1578–1583.

Gunn, L. S., and T. W. R. East, 1954: The microwave properties of precipitation particles. *Quart. J. Roy. Meteor. Soc.,* **80,** 522–545.

Haddad, Z., E. A. Smith, C. D. Kummerow, T. Iguchi, M. R. Farrar, S. L. Durden, M. Alves, and W. S. Olson, 1997: The TRMM ''Day-1'' radar/radiometer combined rain-profiling algorithm. *J. Meteor. Soc. Japan,* **75,** 799–809.

Hitschfeld, W., and J. Borden, 1954: Errors inherent in the radar measurement of rainfall at attenuating wavelengths. *J. Meteor.,* **11,** 58–67.

Iguchi, T., and R. Meneghini, 1994: Intercomparison of single-frequency methods for retrieving a vertical rain profile from airborne or spaceborne radar data. *J. Atmos. Oceanic Technol.,* **11,** 1507–1516.

——, T. Kozu, R. Meneghini, J. Awaka, and K. Okamoto, 2000: Rain-profiling algorithm for the TRMM Precipitation Radar. *J. Appl. Meteor.,* **39,** 2038–2052.

Jaynes, E. T., cited2001: Probability theory: The logic of science. [Available online at http://bayes.wustl.edu/etj/prob.html.]

Kummerow, C., and L. Giglio, 1994: A passive microwave technique for estimating rainfall and vertical structure information from space. Part I: Algorithm description. *J. Appl. Meteor.,* **33,** 3–18.

Marks, C. J., and C. D. Rodgers, 1993: A retrieval method for atmospheric composition from limb emission measurements. *J. Geophys. Res.,* **98,** 14 939–14 953.

Marshall, J. S., and W. H. Palmer, 1948: The distribution of raindrops with size. *J. Meteor.,* **5,** 165–166.

Marzoug, M., and P. Amayenc, 1994: A class of single- and dual-frequency algorithms for rain-rate profiling from a spaceborne radar. Part I: Principle and tests from numerical simulations. *J. Atmos. Oceanic Technol.,* **11,** 1480–1506.

Miller, S. D., G. L. Stephens, C. K. Drummond, A. K. Heidinger, and P. T. Partain, 2000: A multisensor diagnostic satellite cloud property retrieval scheme. *J. Geophys. Res.,* **105,** 19 955–19 971.

Olson, W. S., C. D. Kummerow, G. M. Heymsfield, and L. Giglio, 1996: A method for combined passive–active microwave retrievals of cloud and precipitation profiles. *J. Appl. Meteor.,* **35,** 1763–1789.

Petty, G. W., 1994a: Physical retrievals of over-ocean rain rate from multichannel microwave imagery. Part I: Theoretical characteristics of normalized polarization and scattering indices. *Meteor. Atmos. Phys.,* **54,** 79–99.

——, 1994b: Physical retrievals of over-ocean rain rate from multichannel microwave imagery. Part II: Algorithm implementation. *Meteor. Atmos. Phys.,* **54,** 101–121.

Rodgers, C. D., 1976: Retrieval of atmospheric temperature and composition from remote measurements of thermal radiation. *Rev. Geophys. Space Phys.,* **14,** 609–624.

——, 1990: Characterization and error analysis of profiles retrieved from remote sounding measurements. *J. Geophys. Res.,* **95,** 5587–5595.

Simpson, J., R. F. Adler, and G. R. North, 1988: A proposed Tropical Rainfall Measuring Mission (TRMM) satellite. *Bull. Amer. Meteor. Soc.,* **69,** 278–295.

——, C. Kummerow, W.-K. Tao, and R. F. Adler, 1996: On the Tropical Rainfall Measuring Mission (TRMM). *Meteor. Atmos. Phys.,* **60,** 19–36.

Smith, E. A., X. Xiang, A. Mugnai, and G. J. Tripoli, 1994: Design of an inversion-based precipitation profile retrieval algorithm using an explicit cloud model for initial guess microphysics. *Meteor. Atmos. Phys.,* **54,** 53–78.

Spencer, R. W., H. M. Goodman, and R. E. Hood, 1989: Precipitation retrieval over land and ocean with the SSM/I: Identification and characteristics of the scattering signal. *J. Atmos. Oceanic Technol.,* **6,** 254–273.

Wang, Y., and Coauthors, 1996: Mesoscale model simulations of TRACE A and preliminary regional experiment for storm-scale operational and research meteorology convective systems and associated tracer transport. *J. Geophys. Res.,* **101,** 24 013–24 027.

Wexler, R., 1948: Rain intensities by radar. *J. Meteor.,* **5,** 171–173.

Wilheit, T. T., A. T. C. Chang, M. S. V. Rao, E. B. Rodgers, and J. S. Theon, 1977: A satellite technique for quantitatively mapping rainfall rates over the oceans. *J. Appl. Meteor.,* **16,** 551–560.